nature communications

Article

https://doi.org/10.1038/s41467-025-65344-4

Transient overexpression of hPKM2 in porcine cardiomyocytes prevents heart failure after myocardial infarction

Received: 3 February 2024

Accepted: 10 October 2025

Published online: 24 November 2025

Check for updates

Jiacheng Sun[1,8], Yalin Wu[1,8], Matthew Adjmi[2,3,4,8], Rachel C. Matthews[1], Ann Anu Kurian[2,3,4], Magdalena M. Żak[2,3,4], Jimeen Yoo[2,3,4], Gayatri Mainkar[2,3,4], Hannah Lawless[1], Yu-An Lu[1], Patrick Soon-Shiong[5], Gregory P. Walcott[6], Hesham A. Sadek[7], Jianyi Zhang[1,6] ✉ & Lior Zangi[2,3,4] ✉

The adult mammalian heart lacks the ability to regenerate after injury, contributing to heart failure. No current treatment reactivates heart muscle cell division to prevent this decline. We used a targeted, non-viral modified mRNA system to transiently boost expression of a regenerative enzyme, pyruvate kinase muscle isozyme M2, in heart muscle cells of juvenile and adult pig models after ischemic injury. In juvenile pigs treated one-week post-injury, we observed increased markers of cell division, secretion of protective factors, improved heart function, and reduced scarring two months later. In adult pigs treated immediately after injury, we saw improved heart contractility and less fibrosis one month later. These results show that targeted pyruvate kinase muscle isozyme M2 modified mRNA delivery can stimulate muscle regeneration and functional recovery in both young and adult pig hearts. This approach offers a promising strategy for repairing ischemic injury and preventing heart failure in humans.

After ischemic cardiac injury, non-dividing cardiomyocytes (CMs) die and are replaced by fibrosis and scarring that limit heart function and trigger heart failure (HF), which is the leading cause of death worldwide[1]. To reduce the detrimental effects of ischemic cardiac injury, several strategies – such as tissue engineering[2], cell therapy[3] and gene therapy[4] – have been evaluated, but with limited success. Gene therapies include both viral (e.g., adeno-associated virus (AAV)) and non-viral (e.g., siRNA, shRNA and mRNA) gene delivery methods. modified mRNA (modRNA) is a non-viral gene delivery platform that was used to create the two successful modRNA COVID-19 vaccines[5–7]. modRNA has also been applied in a mouse myocardial infarction (MI) model to promote cardiac regeneration (by inducing remuscularization)[8–10], cardiac protection (by preventing cardiac cell death)[11–13] and cardiovascular regeneration (by promoting angiogenesis in the myocardium)[14–16] post injury. Recent efforts within cardiology have sought to translate modRNA treatments to the clinic. A 2018 paper demonstrated that VEGF-A modRNA enabled cardiovascular regeneration when injected into left ventricle (LV) myocardium one week post ischemic injury in a pig ischemia-reperfusion (I/R) model[15]. VEGF-A modRNA modestly (~5%) improved ejection fraction (%EF) and less cardiac scarring in a juvenile pig I/R model. One year later, Gan et al. showed that VEGF-A modRNA safely produces angiogenesis in humans[17]. In 2023, a phase 2a human clinical trial using VEGF-A modRNA confirmed safety but also indicated low efficacy: VEGF-A modRNA

[1]Department of Biomedical Engineering, School of Medicine and School of Engineering, University of Alabama at Birmingham, Birmingham, AL, USA. [2]Cardiovascular Research Center, Icahn School of Medicine at Mount Sinai, New York, NY, USA. [3]Department of Genetics and Genomic Sciences, Icahn School of Medicine at Mount Sinai, New York, NY, USA. [4]Black Family Stem Cell Institute, Icahn School of Medicine at Mount Sinai, New York, NY, USA. [5]NantRNA, LLC, Wilmington, DE, USA. [6]Division of Cardiovascular Diseases, Department of Medicine, University of Alabama at Birmingham, Birmingham, AL, USA. [7]Division of Cardiology, The University of Arizona College of Medicine, Tucson, AZ, USA. [8]These authors contributed equally: Jiacheng Sun, Yalin Wu, Matthew Adjmi. ✉e-mail: jayzhang@uab.edu; lior.zangi@mssm.edu

failed to form new muscle or promote LV thickness, outcomes that may have led to more significant cardiac repair[18]. Several studies have explored employing protein delivery[19–23], viruses[21,22,24,25] or transgenic mouse models of pro-proliferation genes[26–28] to induce adult CM proliferation and create new muscle.

In 2018, we showed that secreted mutant hFSTL1 modRNA promoted CM proliferation and cardiac repair but also increased immune cell proliferation[8]. To prevent modRNA from activating cell types other than CMs (i.e., immune cells), we designed a CM-specific modRNA translational system (CM SMRTs) that allows modRNA translation only in CMs when delivered naked. CM SMRTs comprises two circuit modRNAs. One is a suppressor gene (either L7AE or Cas6) modRNA carrying CM-specific microRNA (miR) binding sites and the other is a target gene carrying a suppressor gene recognition site (K-motif if the suppressor gene is L7AE and hairpin if the suppressor gene is Cas6). In cardiac cells, miR1 and miR208 are exclusively expressed in CMs, but not in non-CMs, and are upregulated after ischemic injury. Both miRs detrimentally affect the heart in ischemic settings: miR1 causes apoptosis[29] and negatively regulates angiogenesis by modulating VEGFA expression[30], and miR208 supports cardiac fibrosis[31] in the injured heart. When injected naked directly into the heart, CM SMRTs inhibits modRNA translation in cell types that lack miR-1 or miR-208 (i.e., non-CMs) and allows translation only in CMs. We used this system in mice to upregulate mouse Pkm2 (mPkm2), a gene involved in instigating anabolic metabolism, in order to promote CM proliferation and cardiac regeneration post MI. Further, we have shown that mPkm2 CM SMRTs changed the CM metabolic pathway and helped activate the pentose phosphate (PPP) pathway, which generates precursors for synthesizing nucleotides. In parallel, we have demonstrated that mPkm2 attaches to β-catenin in the CM nucleus and boosts cyclin D1 and c-Myc expression in CMs. These changes in CMs expanded their proliferation but did not influence non-CM proliferation. Additionally, when delivered either immediately or two weeks after MI, mPkm2 CM SMRTs improved outcomes after injury. We also determined that, in addition to delivering the vector payload (e.g., Pkm2), CM SMRTs lowered expression of both miR1 and miR208 after MI, thereby providing an additional potential benefit[32]. While our mouse studies presented compelling evidence for applying mPkm2 CM SMRTs to encourage cardiac repair after ischemic injury, it should be noted that because mouse hearts and human hearts differ greatly in size, CM nucleation and heart rate, the beneficial effects of mPkm2 CM SMRTs in mice are not compelling enough for human clinical translation. Yet, Pig hearts serve as a more clinically relevant model for human cardiovascular disease due to their similar size, CM nucleation and biology, heart rates, coronary artery anatomy and absence of extensive collateral circulation. Therefore, using PKM2 CM SMRTs to regenerate pig hearts after ischemic injury may pave the way for human clinical applications to treat HF. Encouraged by previous studies that applied protein, AAV and modRNA gene delivery methods to induce cardiac repair post I/R in pigs[33–35], we wanted to evaluate if mouse or human PKM2 CM SMRTs can trigger CM proliferation and cardiac repair when injected directly into the myocardium immediately or one week after ischemic injury in adult or juvenile pig I/R models.

Here, we show that cardiomyocyte-specific delivery of hPKM2 through the CM SMRTs system promotes cardiomyocyte proliferation, induces angiogenesis, and supports protective paracrine signaling after ischemic injury. In juvenile pigs treated one week after I/R, hPKM2 improves contractile performance, reduces scar formation, and increases vascularization at long-term follow-up. In adult pigs treated immediately after I/R, hPKM2 enhances systolic function, limits fibrosis, and prevents adverse remodeling. Together, these results demonstrate that targeted delivery of hPKM2 modRNA through CM SMRTs achieves remuscularization and functional recovery in large-animal models of I/R injury, supporting its potential as a therapeutic approach to prevent or treat HF.

Results

Naked modRNA distributes broadly in the pig heart after I/R injury

While modRNA has been used to promote cardiovascular regeneration in pigs[15], its biodistribution following direct myocardial injection has not previously been characterized. To evaluate this, we injected the mid-left ventricle (mid-LV) of two juvenile Yorkshire pigs (~35 kg, one male, one female) with either vehicle (sucrose citrate buffer) or naked LacZ modRNA that translates to beta-galactosidase protein, one week after I/R. I/R Injury was incurred for 60 min by left anterior descending (LAD) artery ballon occlusion and reperfusion. Hearts were harvested one week later (two weeks post I/R) and stained with X-gal to detect β-galactosidase activity. LacZ-positive staining was observed extensively in tissue adjacent to the infarct region, with no signal in vehicle controls. Quantification indicated that LacZ expression covered approximately 30% of the LV, thus demonstrating broad regional transfection efficiency surrounding the infracted area (Fig. 1a–c).

CM SMRTs drives CM-specific modRNA expression in the pig heart post I/R

To determine whether CM SMRTs could restrict modRNA translation to CMs in pigs, we injected either nuclear GFP (nGFP) modRNA or nGFP-CM SMRTs into the infarct border zone of juvenile pigs one week after I/R ($n = 2$ per group). Immunostaining for cardiac Troponin T (cTnT), a specific marker for CM, and GFP revealed distinct expression patterns. Conventional nGFP modRNA yielded GFP expression in both cTnT+ (CM) and cTnT- (non-CM cells), with a 2:1 CM-to-non-CM ratio (Fig. 1d–e). In contrast, CM SMRTs achieved near-exclusive CM specificity, with a 16:1 CM-to-non-CM ratio, thereby validating specificity in the pig myocardium (Fig. 1f).

hPKM2 CM SMRTs mediates transient modRNA expression in cardiomyocytes

modRNA translation in the mouse heart was previously found to endure for up to 10 days, peaking after one day and then rapidly declining[9,16,36]. To assess the duration of modRNA expression in pigs, we injected eight juvenile pigs with hPKM2 CM SMRTs one week post I/R and sacrificed animals at 1, 3, 7 or 60 days ($n = 2$ per timepoint). hPKM2 was chosen as a reporter because its absence in adult CMs enables clear detection of modRNA-derived expression. Immunostaining exhibited strong nuclear hPKM2 expression in cardiomyocytes at Day 1, with sustained but decreasing expression that was undetectable on Days 7 and 60. Untreated controls had no observable hPKM2 signal in CMs. These findings confirm that in pigs, like in mice, modRNA expression is transient yet therapeutically relevant for at least one week post-delivery (Fig. 2a–c).

hPKM2 and mPKM2 promote CM proliferation post-injury

Studies of cardiac repair after ischemic injury in mice have demonstrated that stimulating diploid mononuclear CM proliferation can promote cardiac repair[21,26,27,37]. We used two-month-old juvenile Yorkshire pigs (~35 kg, male and female), which have ~10% diploid mononuclear CMs that are comparable to those in non-regenerative adult mammalian hearts. To test whether mPkm2 or hPKM2 CM SMRTs could enhance CM proliferation, we induced I/R injury in eight pigs and injected them one week later with either vehicle, miR1-208 Cas6 modRNA, mPkm2 CM SMRTs or hPKM2 CM SMRTs ($n = 2$ per group). Hearts were harvested seven days after injection. Immunostaining for Ki67 and phospho-histone H3 (PH3) revealed that both mPkm2 and hPKM2 CM SMRTs significantly increased CM proliferation in the border zone, while neither miR1-208 Cas6 modRNA nor vehicle had any impact (Fig. 2d–h). In contrast, none of the treatments elevated these proliferation markers in the remote zone (Fig. 2i–j), a result that further indicates a localized, specific effect of PKM2 in the injected site only.

https://doi.org/10.1038/s41467-025-65344-4

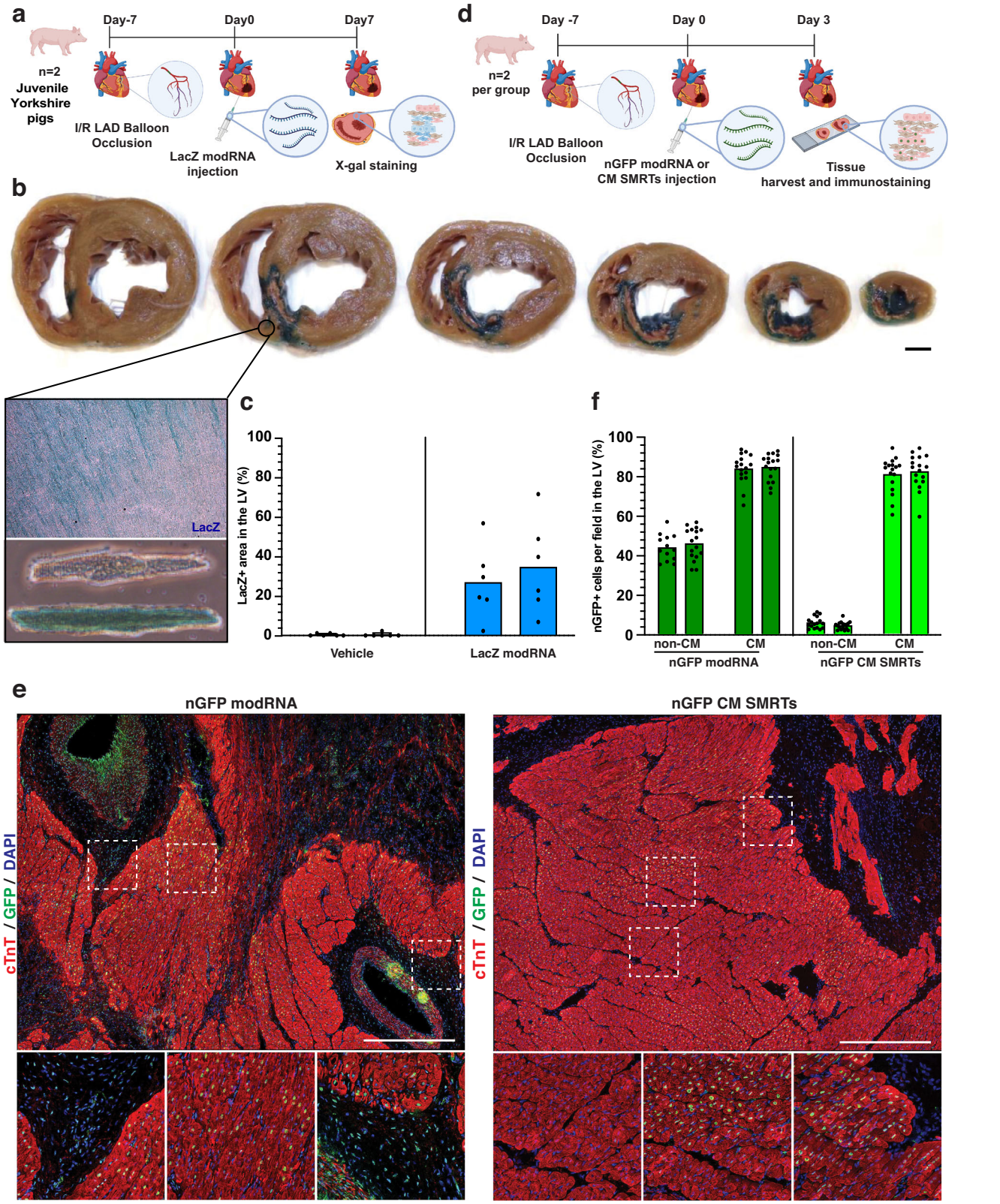

Fig. 1 | CM SMRTs drove efficient, specific protein translation in CMs of porcine hearts after I/R injury. a Experimental timeline to evaluate LacZ modRNA translation efficiency in porcine cardiac cells 7 days post-delivery in an acute I/R model using juvenile Yorkshire pigs. **b** Representative images of X-gal staining of heart slices, cardiac tissue sections and isolated primary CMs from pigs 7 days after LacZ modRNA injection. Scale bar, 2 cm. **c** Quantification of the percentage of LacZ-positive area (blue) relative to LV area. Each dot represents a measurement derived from one image (technical replicate); 8 images were analyzed per pig. $n = 2$ pigs per group. Statistics were not calculated due to insufficient biological replicates. **d** Experimental timeline to demonstrate CM specificity of CM SMRTs. **e** Representative immunofluorescent staining images of nGFP expression in porcine heart cells 7 days post treatment with nGFP modRNA (left) or nGFP CM SMRTs (right). Scale bar, 500 μm. **f** Quantification of the ratios of nGFP-positive CMs and non-CMs under high-power field (40×, 0.64 mm×0.64 mm) in the LV of porcine hearts 3 days after injection. Each dot represents a technical replicate; 18 images were analyzed per pig. $n = 2$ pigs per group. Statistics were not calculated due to insufficient biological replicates. Panels (a&d) Created in BioRender. Zangi, L. (2025) https://BioRender.com/t4rhdsf.

hPKM2 CM SMRTs upregulates angiogenic and cardioprotective targets

Beyond promoting cell cycle activity in CMs, PKM2 has been implicated in angiogenesis through activating paracrine signaling. Our previous studies showed that PKM2 interacts with β-catenin to upregulate c-Myc, a key angiogenic transcription factor[9]. Others have demonstrated that PKM2 can also activate HIF-1α via NF-κB signaling, leading to secretion of VEGFA and other related angiogenic factors[38]. Our RT-qPCR analysis revealed that hPKM2-CM-SMRTs significantly elevated expression of VEGFA, VEGFB, VEGFC, VEGFD, ANG1, leptin and PDGF in the border zone, compared to results from both mPKM2- and control-treated pigs (Fig. 2k). It is important to clarify that, in addition to their recognized roles in cardiovascular regeneration[16,39–44], these upregulated factors also exhibit cardioprotective capabilities[42,45–50]. Moreover, hPKM2 delivery selectively upregulated key PKM2 transcriptional targets, namely HIF-1α, c-Myc and NF-κB (Fig. 2l), in the myocardium seven days post-treatment, a change that is consistent with PKM2 translation and a sustained complex angiogenic gene response. These findings center PKM2 as a key regulatory gene to induce remuscularization, revascularization and cardiac protection post ischemic injury and thus promote cardiac repair, in a large animal model.

Given that both mPKM2 and hPKM2 CM SMRTs increased CM proliferation but only hPKM2 significantly enhanced the expression of angiogenic and cardioprotective secreted factors, we chose to focus only on hPKM2 for long-term therapeutic evaluation. Moreover, our translational goal for this study is to advance toward human clinical application, and using the mouse homolog (mPKM2) in humans could pose immunogenicity risks due to minor antigenic differences[51]. Therefore, we exclusively tested hPKM2 CM SMRTs in a large-animal model of long-term I/R injury.

hPKM2 CM SMRTs restores cardiac function and reduces scar size

To assess therapeutic efficacy in a chronic I/R model, we injected either hPKM2 CM SMRTs or vehicle into 20 juvenile Yorkshire pigs one week after injury ($n = 10$ per group, weight ~35 kg, male and female, randomly assigned). Cardiac function was monitored by echocardiography (Echo) at several time points (Days −7, 0, 10, 56) and cardiac MRI (MRI) at Day 56 (Fig. 3a). By the day of treatment (Day 0), both groups exhibited decreased cardiac function (% ejection fraction (%EF) ~ 34%), thus confirming injury. In the vehicle-treated group, cardiac function continued to deteriorate, reaching 32.1 %EF and 15% fractional shortening (%FS) by Day 56. In contrast, the hPKM2 group exhibited progressive and sustained improvement, with %EF increasing to 54.1 and %FS to 27.5 by Day 56—levels consistent with preserved or near-normal heart function (Fig. 3b–d). Notably, Echo of hPKM2-treated pigs uncovered no significant differences in %EF and %FS between Days 10 and 56, suggesting stabilized improvement that took place in the first days after hPKM2 CM SMRTs delivery.

All vehicle-treated pigs, but none of the hPKM2-treated pigs, met criteria for heart failure with reduced ejection fraction (HFrEF)[52] by Day 56 (Fig. 3b–d and Supplementary Fig. 1). Confirming these findings, MRI showed significantly improved cardiac function in hPKM2-treated animals at endpoint: %EF rose to 50.3 vs. 31.7 in controls (Fig. 3e–f). Stroke volume was elevated, while end-systolic volume decreased significantly in the hPKM2 group; end-diastolic volume remained unchanged (Fig. 3g–i). Strain analysis indicated enhanced regional wall motion in the mid-LV–the injection site–with more radial strain (εrr) and LV wall thickening (LVWT) in hPKM2-treated pigs (Fig. 3j–m and Supplementary Fig. 2a, b). Histological analysis of hearts sectioned from apex to base revealed significantly smaller infarct area in hPKM2-treated pigs, particularly in mid and apical segments (Fig. 3n and Supplementary Fig. 4a, b). Late gadolinium-enhanced cardiac MRI (LGE-cMRI) performed before and after treatment demonstrated significant decreases in infarct volume and scar size in hPKM2-treated hearts (Fig. 3o–q). LGE-cMRI analysis also showed smaller infarct core (white zone) and peri-infarct area (gray zone) (Supplementary Fig. 5), results that suggest improvements in both structural integrity and tissue viability.

hPKM2 promotes angiogenesis and CM renewal without adverse effects

In order to evaluate vascular and cellular remodeling, we analyzed hearts collected 56 days post injection. Immunostaining revealed significantly more luminal structures containing endothelial cells (CD31 +), smooth muscle cells (αSMA +) and pericytes (NG2 + / CD31 +) in hPKM2-treated myocardium compared to vehicle (Fig. 4a–g). That no significant difference in immune cell infiltration (CD45 +) was observed after hPKM2 treatment (Fig. 4h–i) indicated more mature capillaries with no increase in chronic inflammation. Additionally, CM analysis showed significantly smaller CM cross-sectional areas in the hPKM2 group (Fig. 4j–k) and a greater proportion of mononuclear CMs, without expansions of either bi- or multi-nucleated CMs (Fig. 4l), results that suggest cell renewal rather than hypertrophy. To assess the persistence of CM proliferation, we stained for Ki67 at Day 56 and found no differences between groups, thus indicating the proliferative response was transient and controlled (Fig. 4m–n). To determine electrical safety, programmed electrical stimulation (PES) was performed on Day 56. The frequency of sustained and non-sustained ventricular arrhythmias was similar between groups (Fig. 4o–p and Supplementary Fig. 6). This shows hPKM2 CM SMRTs did not increase arrhythmogenic risk. Collectively, these results demonstrate that hPKM2 CM SMRTs promotes cardiac regeneration and vascular remodeling without causing adverse effects.

hPKM2 CM SMRTs improves cardiac function and capillary density in adult Sinclair pigs

To assess the translational relevance of hPKM2 CM SMRTs, we tested its therapeutic effects in adult Sinclair minipigs (~1 year old, ~35 kg). Given the heightened procedural risk of balloon angioplasty in this strain, due to their smaller and more intricate coronary vasculature[53], we induced I/R via open-chest LAD occlusion and immediately delivered hPKM2 CM SMRTs or vehicle ($n = 3$ vehicle; $n = 4$ hPKM2) via direct epicardial intramyocardial injection. By 28–29 days post-injury, Echo revealed significantly improved cardiac contractility in hPKM2-treated pigs, with a 16.7% increase in %EF and 9.7% increase in %FS compared to controls (Fig. 5a–c and Supplementary Fig. 7). Hearts collected at endpoint and then sectioned showed substantially smaller scars in hPKM2-treated animals (Fig. 5d, e). Border zone histology comparing hearts from hPKM2-treated animals to those from controls revealed a reduction in CM cross-sectional area (Fig. 5f, g) and an increased proportion of mononuclear CMs (Fig. 5h), changes that suggest regenerative remodeling via CM proliferation. Proliferation markers Ki67 and PH3 showed no differences between groups at this time point (Day 29, Fig. 5i, j), thus indicating that hPKM2-induced cell cycle activity had subsided, which is consistent with a transient, regulated proliferative response. Vascular analysis demonstrated, in alignment with our juvenile pig results shown in Fig. 4), a significant increase in luminal structures containing CD31+ endothelial cells (Fig. 5k, l), αSMA+ smooth muscle cells (Fig. 5m, n) and CD31 + /NG2+ pericytes (Fig. 5o, p), while CD45+ immune cell infiltration remained unchanged (Fig. 5q, r). These results highlight the CM pro-proliferative role and angiogenic potential of hPKM2 and confirm its safety in an adult large-animal model. Collectively, these studies support the clinical promise and safety of hPKM2 CM SMRTs for cardiac repair post ischemic injury.

Discussion

The adult mammalian heart has a limited ability to regenerate after injury. Both mice and pigs lose cardiac regenerative capacity within the

https://doi.org/10.1038/s41467-025-65344-4

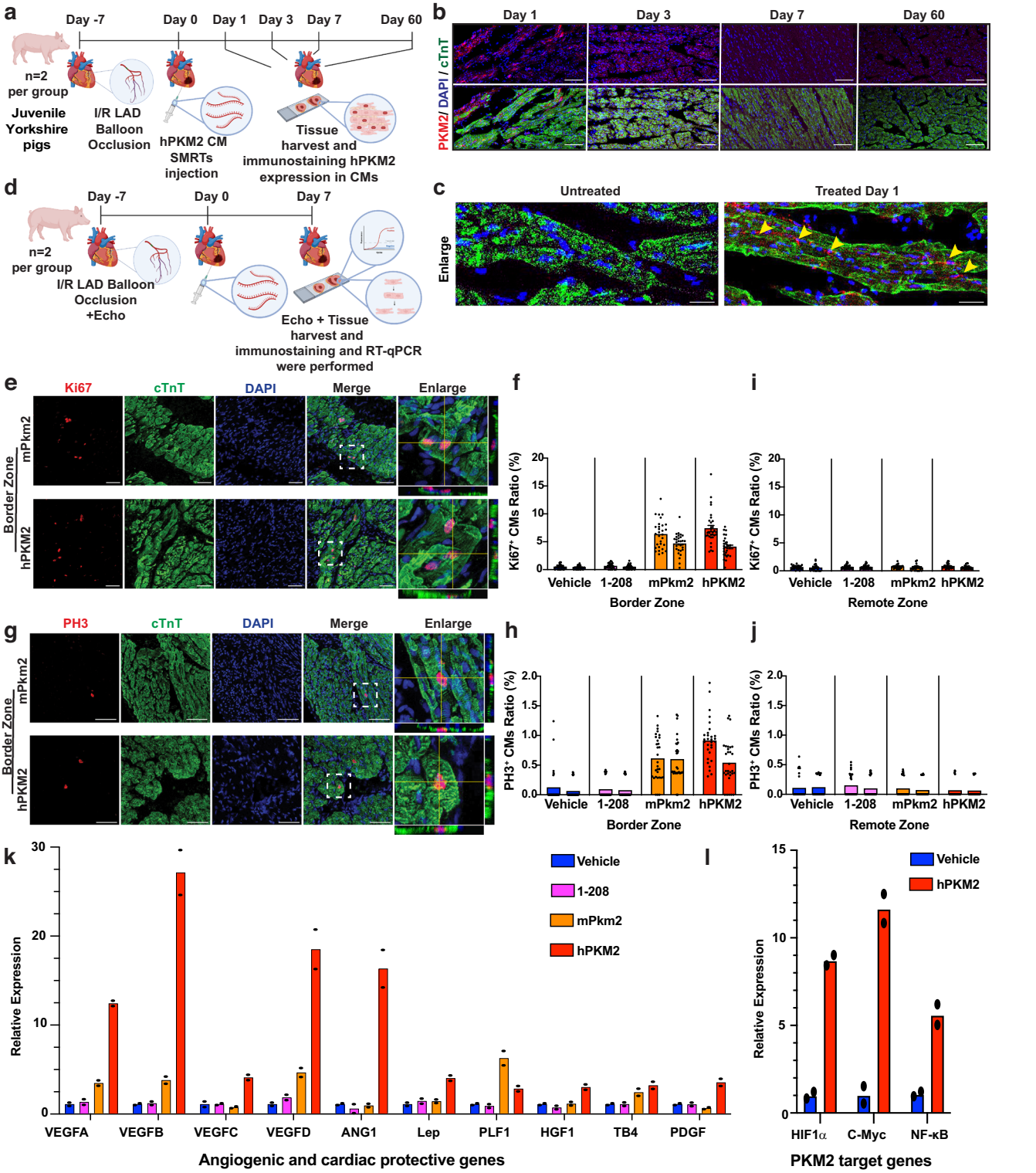

Fig. 2 | Human PKM2 CM SMRTs promoted CM cell cycle activity and expression of both angiogenic paracrine factors and cardiac protective genes in a porcine I/R model. a Experimental timeline to evaluate the pharmacokinetics of hPKM2 CM SMRTs. (**b&c**) Representative images (**b**) of hPKM2 expression in CMs from border zone. Yellow arrows in the enlarged images (**c**) show nuclear hPKM2 expression in CMs. **d** Experimental timeline to evaluate the effects of mPkm2 and hPKM2 CM SMRTs on CM cell cycle activity and secretion of angiogenic paracrine factors 7 days post-delivery in an acute I/R model using juvenile Yorkshire pigs. Representative images of proliferation marker Ki67 (**e**) and quantification of Ki67 in CMs from border zone (**f**). Representative images of proliferation marker G2/M phase marker PH3 (**g**) and quantification of PH3 in CMs from border zone (**h**). Quantification of Ki67 (**i**) or PH3 (**j**) in CMs from remote zone. RT-qPCR quantification of different angiogenic paracrine factors and cardiac protective genes (**k**) or PKM2 target genes (**l**) in the border zone after treatments versus vehicle. For quantifications depicted in subfigures (**f**, **h**, **i**, **j**) each dot represents a measurement derived from a single image (technical replicate) obtained from stained sections from each pig. Thirty images were analyzed per pig. *n* = 2 pigs per group. Scale bars: (b,e,g) = 50 μm; (**c**) = 20 μm. Panels (**a**, **d**) Created in BioRender. Zangi, L. (2025) https://BioRender.com/7y4vgj0.

https://doi.org/10.1038/s41467-025-65344-4

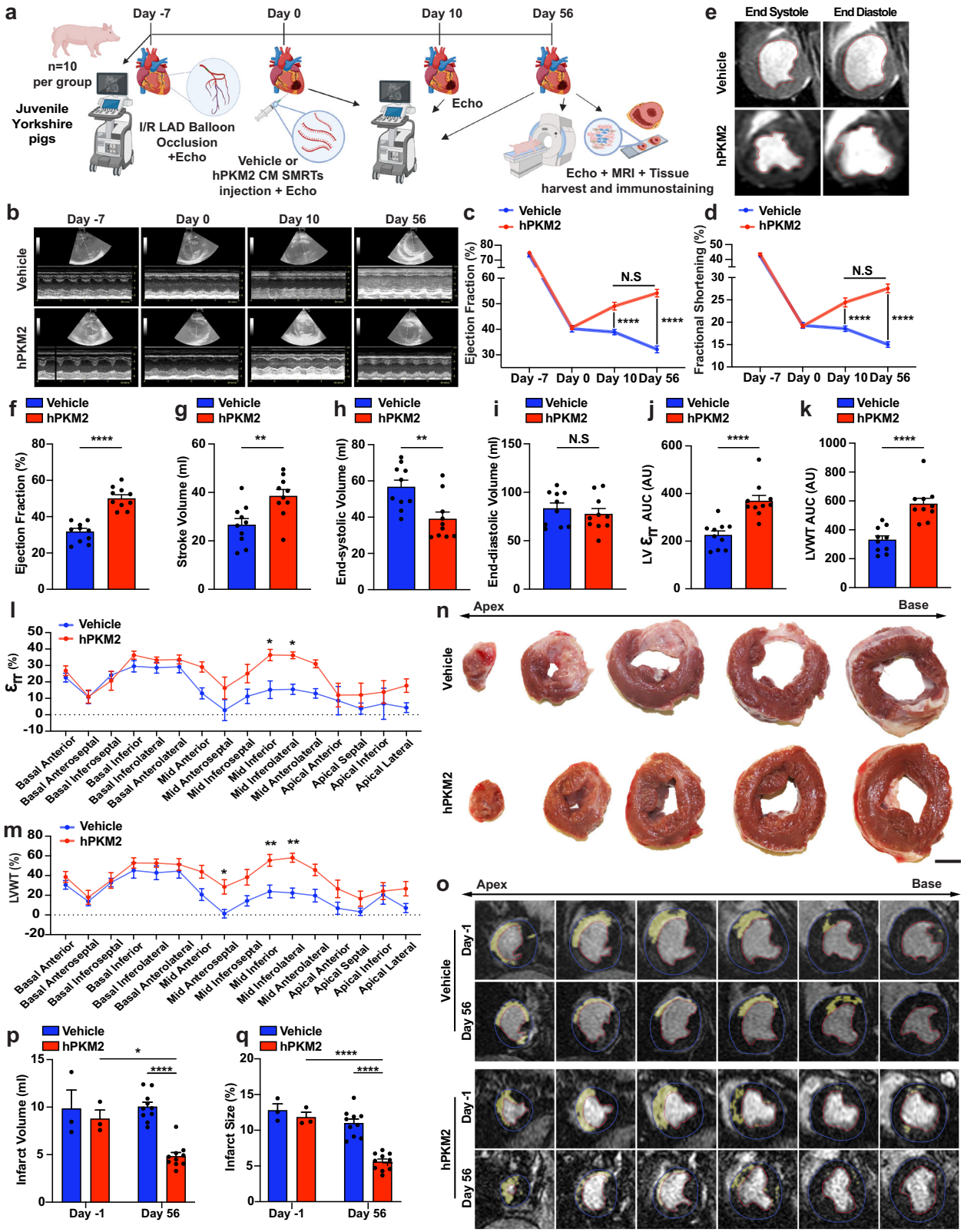

first week of life as their mononuclear diploid CMs lose proliferation capacity[54,55]. Many efforts have tried to reactivate CM proliferation in adult hearts as a way to repair damage from ischemic heart disease (IHD), but progress towards clinical translation has been slow. Delivery method has been one major barrier. Proteins are limited by their short half-life and inability to deliver transcription factors into relevant cellular locations. Viral vectors incur safety concerns, cannot be temporally controlled and are readily recognized by the innate and adaptive human immune system[56,57].

Several recent studies have attempted to promote mononuclear CM division to induce cardiac repair in porcine I/R models. In 2019, Gabisonia et al. showed that delivering AAV carrying human miR-199a can stimulate repair in infarcted pig hearts; however, subsequent persistent and uncontrolled expression of miR-199a caused sudden

Fig. 3 | Intramyocardially injected hPKM2 CM SMRTs improved cardiac function and reduced infarct size in an I/R model using Juvenile Yorkshire pigs. **a** Experimental timeline to evaluate cardiac function and outcome in an acute I/R porcine model using juvenile Yorkshire pigs. Echocardiographic images (**b**) obtained from pigs in the hPKM2 CM SMRTs and vehicle groups before balloon occlusion (Day −7), before injection (Day 0), and 10 and 56 days after intervention. These images were used to calculate (**c**) %EF and (**d**) %FS. Cardiac magnetic resonance imaging (**e**, cMRI) was performed on Day 56 and used to calculate (**f**) %EF, (**g**) stroke volume, **h** end-systolic volume, and (**i**) end-diastolic volume. Sixteen-segment curves corresponding to (**j**) radial strain (εrr) and (**k**) LV wall thickening (% LVWT) on Day 56 after intervention. Calculation of the (**l**) area under the curve (AUC) in arbitrary units for ε_{rr} and (**m**) LVWT at different heart segments. (**n**) Representative images of LVs collected on Day 56 and cut into five circular sections from the apex to the base (see Supplementary Fig. 4a for all collected images). Late gadolinium enhancement cardiac MRI (LGE-cMRI) images were obtained from pigs 1 day before (Day −1) and 56 days after (Day 56) injection. (**o**) Representative LGE-cMRI images from one vehicle-treated and one hPKM2 CM SMRTs-treated animal, acquired on Day −1 and Day 56. The endocardium is contoured in red, the epicardium in blue, and the infarct area in yellow. LGE-cMRI images were used to calculate infarct (**p**) volume and (**q**) infarct size. $n = 10$ biological replicates (pigs) per group unless otherwise stated; unit of study = pig. For (**c**, **d**), data points represent group means at each time point; error bars indicate SEM from $n = 10$ pigs/group. For (**f**–**k**), each dot represents one pig ($n = 10$/group); data are presented as mean ± SEM. For (**l**, **m**), data points represent group means for each heart segment; error bars indicate SEM from $n = 10$ pigs/group. For (**p**, **q**), each dot represents one pig; $n = 3$/group at Day −1 and $n = 10$/group at Day 56; data are presented as mean ± SEM. Scale bar = 2 cm. Two-way ANOVA with Tukey's multiple comparison test for (**c**, **d**, **l**, **m**, **p**, **q**); unpaired two-tailed *t*-test for (**f**–**k**). $^{*}P < 0.05$; $^{**}P < 0.01$; $^{****}P < 0.0001$; N.S., not significant. For additional statistical information, see Supplementary data 1. Panel (**a**) Created in BioRender. Zangi, L. (2025) https://BioRender.com/t1c39vu.

arrhythmic death in most of the treated pigs within two months[58]. In 2020, Baehr et al. conducted a one-month study demonstrating that injecting Agrin protein immediately after I/R is sufficient to reduce cardiac remodeling and improve cardiac function[34]. In 2021, Liu et al. established that administering AAV carrying small hairpin RNAs (shRNA) to inhibit the Hippo pathway Salvador (Sav) gene after I/R resulted in tissue renewal and improved cardiac function in farm pigs[33]. While these studies provide important proof-of-concept data, they nevertheless rely on protein and viral delivery. Protein-based therapies pose challenges related to the heart's unique structure and function[59]; further, the large sizes, short half-lives and low capacities for cellular entry decrease the efficiency of protein delivery. AAV-based approaches are limited by a lack of temporally controlled expression as well as the presence of anti-AAV neutralizing antibodies in humans. Furthermore, AAV has been shown to present low-frequency integration into the host genome, probably due to mediation by the host's DNA-modifying enzymes, a process that may lead to tumorigenic formation in the liver[56,57].

Unlike the methods detailed above, the modRNA approach is a safe, transient and non-immunogenic gene delivery system. Until now, modRNA has been successfully used in a porcine I/R model to induce cardiac regeneration, but not CM proliferation[15]. In the pre-clinical pig study using VEGF-A modRNA, 1 or 10 mg of naked VEGF-A modRNA was directly injected into infarcted pig myocardium one week post I/R[15]. In a phase 2a clinical trial, 1 or 3 mg VEGF-A modRNA was directly injected into the myocardium of patients undergoing coronary bypass grafting. This study confirmed intracardiac modRNA delivery to be safe and tolerable in humans[18]. The main limitation of the VEGF-A modRNA clinical trial was its narrow capacity for cardiac repair. VEGF-A as a secreted factor has limited effects compared to a transcription factor, like PKM2, that has several functions involved in multiple biological pathways. Our present study shows that hPKM2 modRNA, delivered selectively to CMs via our CM SMRTs system, can promote CM proliferation, cardiovascular regeneration and cardiac protection in a porcine I/R model, without triggering inflammation or arrhythmias.

In this study, we confirmed, for the first time, that delivering 6 mg of modRNA leads to widespread protein expression in approximately 30% of the LV area and that by using nGFP CM SMRTs (contain 6 mg nGFP modRNA and 1.5 mg Cas6 modRNA) we were able to restrict expression almost entirely to CMs (Fig. 1). We have previously shown[60] that modRNA delivered using self-assembling LNPs enabled higher translation than naked modRNA (~40% more translation in the heart) when injected directly into the heart. However, while naked modRNA expression occurred exclusively at the injection site, encapsulated modRNA allows translation in unwanted organs (e.g., the liver). Therefore, we prefer naked modRNA over LNP-encapsulated modRNA for delivery to the heart.

We have previously shown that mPKM2 modRNA enables transient protein expression, thereby changing CM metabolism and directly activating pro-proliferative genes in the CM nucleus. Indeed, we determined that mPKM2 modRNA injected immediately or two weeks after MI supports cardiac repair and angiogenesis[9]. Other groups have reported similar therapeutic effects of PKM2 in the contexts of mouse, rat and zebrafish cardiac injury[61–63]. Our prior work has also indicated that overexpression of pro-proliferative genes such as Yap, caErbb2, Cyclin D1 or c-Myc elevates endogenous PKM2 mRNA expression in CMs[9].

Our current study found that, mechanistically, hPKM2 modRNA activated transcriptional programs that promote both vascular regeneration[16,41,42] and cardiac protection[48,49] (Fig. 2k). We saw increased levels of the PKM2 targets HIF-1α, c-Myc and NF-κB in the myocardium by Day 7 (Fig. 2l). PKM2 and HIF-1α are involved in a positive feedback loop under hypoxic conditions: HIF-1α stabilizes and activates PKM2 transcription by binding to hypoxia response elements in its promoter. In turn, PKM2 translocates to the nucleus and coactivates HIF-1α, thus amplifying the hypoxic response[38,64,65]. Elevated HIF-1α has been shown to upregulate angiogenic factors like VEGFA under ischemic conditions[66]. c-Myc, a direct PKM2 target, drives CM cell cycle activity[9,67] and is required for proper coronary vascular formation[68]. NF-κB activation contributes to angiogenic cytokine expression and vascular growth[69]. Together, these factors can explain the proliferation, vascular remodeling and cardiac protection provided by hPKM2 treatment.

Although both mouse and human PKM2 boosted CM proliferation markers, only hPKM2 also upregulated the broader angiogenic and cardioprotective gene panel. Although hPKM2 shares 519 of mPKM2's 531 amino acids, the human protein has 74 more amino acids which may play a role in its ability to induce angiogenesis in the pig heart after ischemic injury.

Overall, our findings demonstrate that a single administration of hPKM2 CM SMRTs one week after ischemic injury can induce sustained functional and structural improvements in the heart in juvenile pigs. These benefits persisted through seven weeks, with evidence of regeneration and improved cardiac function. Importantly, CM proliferation was transient and controlled, without signs of immune activation or arrhythmia, thus underscoring the advantages of the modRNA approach. We observed a similar therapeutic pattern in adult pigs after a single administration of hPKM2 immediately after I/R. The adult pig model more accurately reflects the clinical population affected by IHD. Taken together, these results suggest that hPKM2 CM SMRTs can effectively trigger cardiac repair and prevent HF.

It is worth emphasizing that our hPKM2 CM SMRTs approach avoids the safety concerns presented by other delivery methods. For example, AAV-based gene therapies to induce CM proliferation and cardiac repair post I/R risk immune response activation, genomic integration and uncontrolled CM proliferation[33,58,70], whereas our transient modRNA delivery system has a strong safety profile. To date,

https://doi.org/10.1038/s41467-025-65344-4

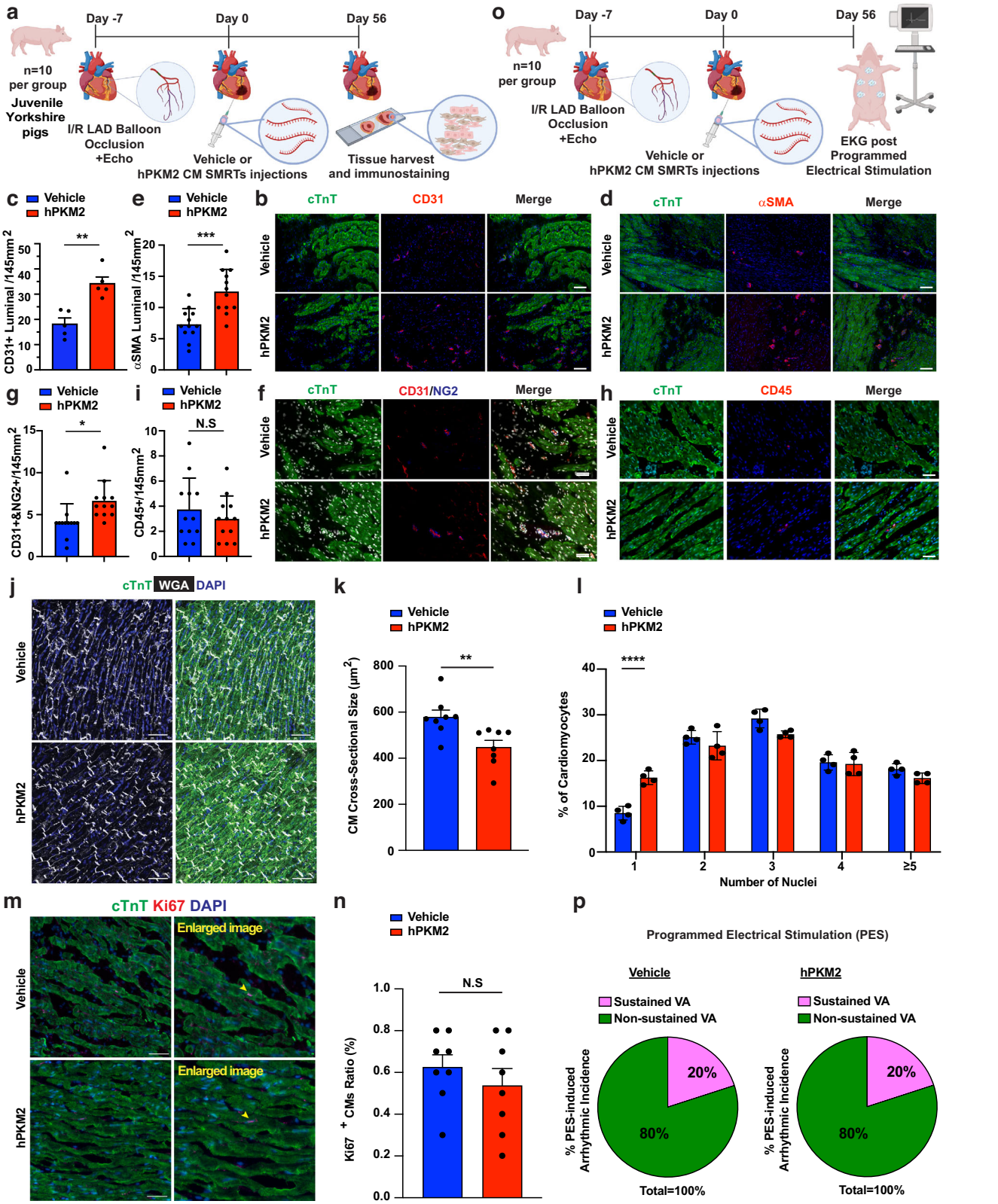

modRNA has been administered safely via COVID-19 vaccines to millions of people[6], and our CM SMRTs platform builds on that success by enabling targeted expression of a potent transcription factor in CMs without provoking immune responses or risking DNA integration. As we here present, hPKM2 delivery promotes CM proliferation and induces cardioprotective and pro-angiogenic gene programs, resulting in thicker ventricular walls, improved function and prevention of heart failure—all without triggering arrhythmias. Notably, while a prior VEGF-A modRNA pig study yielded only modest functional gains (~5% EF improvement), our study, using a similar design, achieved more than fourfold greater benefit (22.5%), a result that highlights the therapeutic potential of hPKM2-CM-SMRTs for regenerative cardiac repair.

This study has several limitations. First, it is unclear to what extent the beneficial effects of hPKM2 are due to creating new muscle versus

Fig. 4 | hPKM2 CM SMRTs promoted angiogenesis, expanded mononuclear CM populations, reduced cardiomyocyte size and did not increase the risk of arrhythmia. a Experimental timeline to evaluate capillary density, immune cell infiltration, CM size, CM proliferation and number of CM nuclei 56 days post treatment in an I/R model using juvenile Yorkshire pigs ($n = 10$ for vehicle and 10 for hPKM2 CM SMRTs). For graphs depicted in subfigures (**c**, **e**, **g**, **i**, **k**, **n**), each dot represents a measurement from one technical replicate (image) obtained from stained sections from each pig. The number of technical replicates varied by staining method and is indicated for each relevant panel: (**c**) = 5; (**e**, **g**, **i**) = 12; **k**, **n** = 8. **b**–**h** Representative images of capillary density evaluation using blood vessels immunostaining of PECAM-1/CD31 (**b**) and quantification of luminal structure per area (145mm2, **c**). Smooth muscle cells immunostained with αSMA (**d**) and quantification of luminal structure per area (**e**); pericytes immunostained with NG2+ and CD31+ (**f**) and quantification of luminal structure per area (**g**); immune cell infiltration immunostained with CD45+ (**h**) and quantification of CD45+ cells per area (**i**) in border zone tissue at 56 days post injection. All slides were counterstained with CM marker (cTnT, green) and for nuclei (DAPI, blue or white in **f**). Representative images (**j**) of border zone CMs stained with cTnT and wheat germ agglutinin (WGA) to visualize CMs and borders. Nuclei were counterstained with DAPI. Quantification of CM cross-sectional area (**k**) and percentage of CM nucleation (**l**) on Day 56. For (**l**), values represent the average proportion of CMs with 1, 2, 3, 4, or ≥5 nuclei calculated per pig from 10 images, then averaged across groups ($n = 10$ pigs per group); data are presented as mean ± SEM. Representative images of Ki67 proliferation marker (**m**) in the border zone 56 days after delivery of hPKM2 CM SMRTs. **n** Quantification of Ki67-positive CMs from the border zone. **o** Experimental timeline to evaluate ventricular arrhythmia (VA) 56 days post treatment in an I/R model using juvenile Yorkshire pigs. **p** Programmed electrical stimulation (PES) was performed in porcine hearts before sacrifice on Day 56. Hearts were paced at 400 ms with additional stimuli provided at progressively shorter intervals; PES was halted immediately after a VA episode occurred. The percentage of sustained VA (lasted ≥15 heart beats) and non-sustained VA (lasted <15 heart beats) in vehicle- or hPKM2 CM SMRTs-treated animals are shown in pie graphs ($n = 10$). Scale bar, 50 μm for (**b**, **d**); 20 μm for (**f**, **h**, **j**, **m**). Data are presented as mean ± SEM. Unpaired two-tailed t-test. N.S., not significant; $^{**}P < 0.01$; $^{***}P < 0.001$; $^{****}P < 0.0001$. For additional statistical information, see Supplementary data 1. Panels (**a**, **o**) Created in BioRender. Zangi, L. (2025) https://BioRender.com/i26hsg7.

protecting injured muscle or improving angiogenesis. We assume that all three mechanisms synergistically support cardiac repair. Second, delivering modRNA into the heart via open chest surgery, although previously used in humans[18], is not an ideal delivery route. Catheter-based administration, which would be more clinically relevant, was not feasible in the present study due to practical constraints. Similar to the AAV delivery method in a previous pig study[33], catheter-based approaches may lead to safer, more reproducible delivery in future work. Moreover, developing targeted lipid nanoparticles (LNPs) for modRNA delivery could create a cardiotropic, minimally invasive gene delivery system that will combine the strength of both LNPs and CM SMRTs[71]. Third, our study evaluated hPKM2 CM SMRTs delivery both immediately and one week after I/R injury (Figs. 3–5). Although these time points provide important proof-of-concept evidence, additional studies at later intervention windows (e.g., one month after ischemic injury, when remodeling is completed) would better reflect patient scenarios. Additionally, the number of adult Sinclair pigs was limited, though the findings support reproducibility across large animal studies through their alignment with those in the juvenile Yorkshire model. Addressing these limitations may shed light on the mechanism of action and therapeutic promise of using hPKM2 CM SMRTs to not only prevent HF but also treat it, while further strengthening the translational relevance of our model. Importantly, our work seeks to use hPKM2 CM SMRTs in human clinical settings to overcome HF and reduce associated mortality.

Methods

Animal care

All experiments and procedures involving animals were approved by the Institutional Animal Care and Use Committee (Animal Protocol Number 20216) of the University of Alabama at Birmingham and were consistent with the Guidelines for the Care and Use of Laboratory Animals published by the US National Institutes of Health (2011). The data, analytic methods and study materials have been or will be made available to other researchers for purposes of reproducing the results or replicating the procedures, and the authors are responsible for maintaining availability. All reporting complies with the ARRIVE guidelines. Both male and females were included in our large animal experiments; sex disaggregated numbers are provided in Supplementary data 1.

modRNA synthesis

Modified mRNAs were transcribed in vitro from plasmid templates containing open reading frame sequences (Supplementary Table 1) via an in vitro transcription kit (MEGAscript T7 Kit, Invitrogen) and a customized ribonucleotide blend of CleanCap Reagent AG, m7G(5′) ppp(5′)(2′OMeA)pG (TriLink Biotechnologies), guanosine triphosphate (GTP; Invitrogen), adenosine triphosphate (ATP; Invitrogen), cytidine triphosphate (CTP; Invitrogen) and N1-methylpseudouridine-5′-triphosphate (TriLink Biotechnologies) as described previously[72]. mRNA was then purified with a Megaclear kit (Invitrogen), quantitated by Nanodrop (Thermo Scientific), concentrated with Amicon Ultra-2 30k Centrifugal Filters (UFC203024, Millipore) and resuspended in a biocompatible sucrose-citrate buffer for in vivo transfection[15].

Juvenile Yorkshire pig I/R model and modRNA injection

This study used Yorkshire swine (both female and male, ~30 kg, ~10 weeks old; Valley Brook Research, Madison, GA). Myocardial infarction was induced by balloon angioplasty. ModRNAs were administered by direct myocardial injection during open chest surgery one week after MI. In both surgical procedures, pigs were sedated with telazol/xylazine (4.4 mg/kg body weight), intubated, anesthetized with inhaled 2% isoflurane and ventilated with a respirator to maintain anesthesia. To induce myocardial infarction, an 8 F sheath was inserted in the left common carotid artery, and then a 7 F coronary guiding catheter was advanced through the carotid artery and ascending aorta to the ostium of the left main coronary artery. Next, a 3 mm angioplasty balloon was positioned in the left anterior ascending artery immediately distal to the second diagonal branch and then inflated for 60 min. Absence of the distal flow of contrast indicating coronary occlusion was observed. To administer modRNA, a median sternotomy was performed, and the therapeutic (mPkm2 CM SMRTs, hPKM2 CM SMRTs, miR1-208 Cas 6 modRNA or delivery vehicle) was injected into five sites in the border zone of the injured myocardium one week after I/R injury. The chest was then closed in layers. After both procedures were completed, pigs were transferred to the intensive care unit for monitoring. Pigs received subcutaneous injections of buprenorphine ER (0.24 mg/kg; ZooPharm, Laramie, WY) at the time of surgery and either oral or intramuscular injections of carprofen (4 mg/kg; Rimadyl, Zoetis, Troy Hills, NJ) QD for 2 days following surgery.

Adult Sinclair minipig I/R model and modRNA injection

Adult Sinclair minipigs (both female and male, ~35 kg, ~1-year-old; Valley Brook Research, Madison, GA) were anesthetized with inhaled 2% isoflurane, intubated and ventilated with a respirator. A center thoracotomy was performed, and the LAD coronary artery distal to the 2nd diagonal was ligated with 4.0 polypropylene sutures for 60 min before reperfusion; then, the animals were randomly assigned to treatment with either hPKM2 CM-SMRTs (6 mg ktm-hPKM2 and 1.5 mg miR1/208RE-L7Ae in 1 mL sucrose-citrate buffer, $n = 4$) or delivery

https://doi.org/10.1038/s41467-025-65344-4

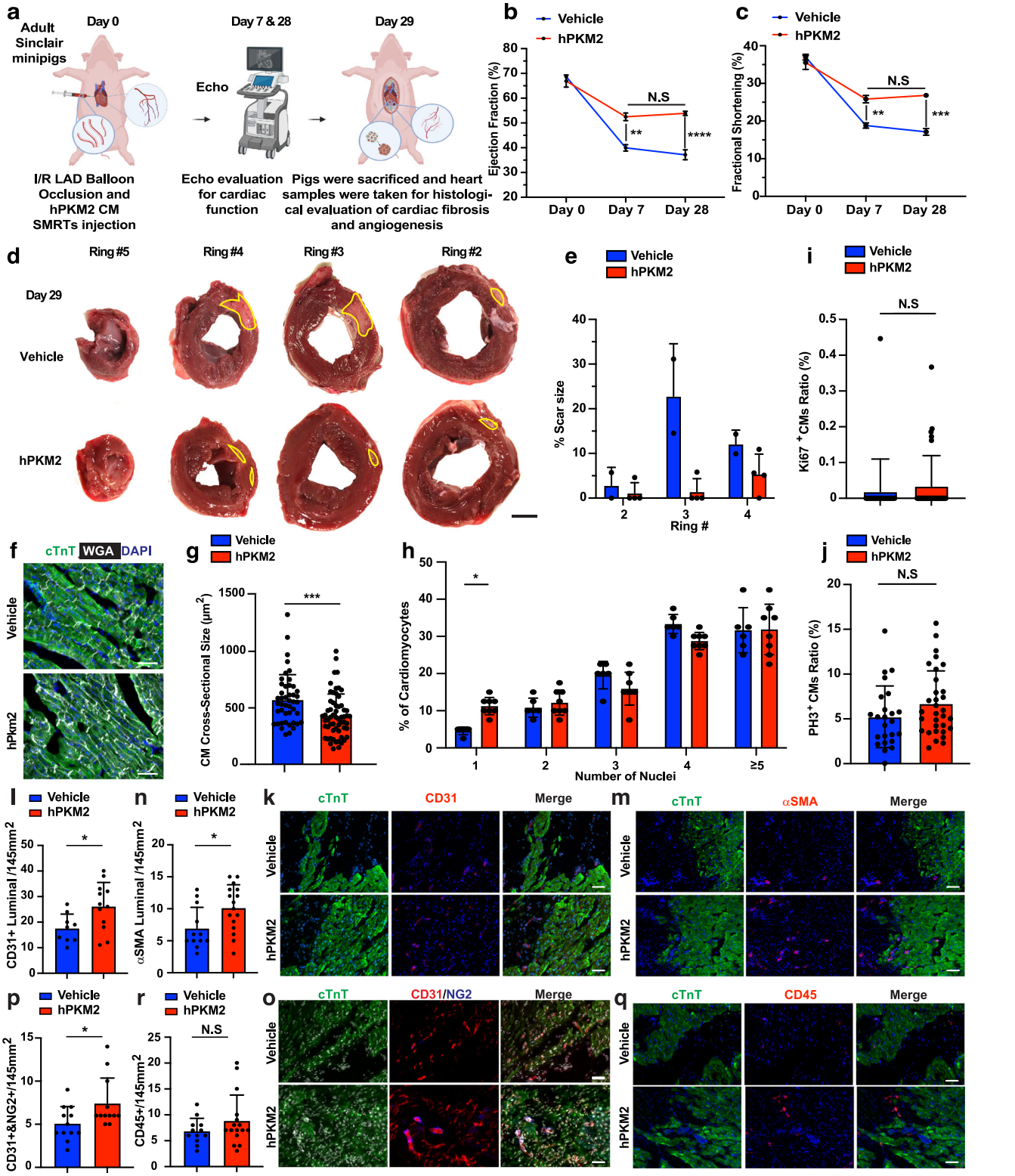

vehicle (1 mL sucrose-citrate buffer, $n = 3$). The hPKM2 CM-SMRTs doses were calculated by dividing the mouse dose by 11.18, as indicated in the US FDA publication "Estimating the Maximum Safe Starting Dose in Initial Clinical Trials for Therapeutics in Adult Healthy Volunteers" (https://www.fda.gov/media/72309/download) and injected immediately after reperfusion into five sites in the border zone of the injured myocardium. After treatment, the chest was closed in layers, and the animals were allowed to recover. Animals received subcutaneous injections of buprenorphine SR (0.24 mg/kg; Buprenex, Rupkitt Benckiser Pharmaceuticals Inc.) every 12 h for up to 3 days and intramuscular injections of carprofen (4 mg/kg; Rimadyl, Zoetis) every 24 h for up to 2 days after surgery.

Histological and immunofluorescence analyses

Pig hearts were explanted at different time points as indicated in manuscript figures. Hearts were washed in cold natural saline, then weighed. Cardiac tissue from the infarct zone and remote zone was dehydrated in 30% sucrose (in PBS) at 4 °C overnight, embedded in

Fig. 5 | Intramyocardially injected hPKM2 CM SMRTs improved cardiac function and reduced infarct size in an adult Sinclair minipig I/R model. **a** Experimental timeline to evaluate cardiac function at different time points, scar formation, capillary density, immune cell infiltration, CM size, CM proliferation and numbers of CM nuclei 29 days post treatment in an acute I/R model using adult Sinclair pigs ($n = 2$ for vehicle and $n = 4$ for hPKM2 CM SMRTs). Echocardiographic images were used to calculate (**b**) %EF and (**c**) %FS. **d** Representative images of LVs collected on Day 29 and cut into four circular ring sections from the apex to the base. **e** Quantification of total scar size in all cardiac rings from the two treated groups. **f** Representative border zone CMs stained with cTnT and WGA, with nuclei counterstained by DAPI. Quantification of CM cross-sectional area (**g**) and multinucleation (**h**). For (**h**), values represent the average proportion of CMs with 1, 2, 3, 4, or ≥5 nuclei calculated per pig from 10 images, then averaged across groups. **i** Quantification of Ki67+ CMs in the border zone (**j**) Quantification of PH3+ CMs in the border zone. Representative immunostaining of PECAM-1/CD31 (**k**), αSMA (**m**), NG2/CD31 (**o**), and CD45 (**q**) with quantification of luminal structures or immune cells (**l**, **n**, **p**, **r**). For quantifications: in (**g**), each dot represents a single CM measurement (15 cells per pig); in (**i**, **j**), each dot represents a ratio derived from 8 images per pig; in (l), images from all pigs were analyzed (12 total images per group), and each dot represents one image; in (**n**), 4 images per pig were analyzed; in (**p**), 12 images per group; and in (**r**), 4 images per pig. Biological replicates were $n = 3$ for vehicle and $n = 4$ for hPKM2 CM SMRTs across all analyses, except panels (**d**, **e**), where 2 vehicle hearts were available. Scale bar = 20 μm for (**f**); Scale bar = 50 μm for (**k**, **m**, **o**, **q**). Data are presented as mean ± SEM. Two-way ANOVA with Tukey's multiple comparison test for (**b**, **c**); unpaired two-tailed t-test for (**e**, **g**, **h**, **j**, **l**, **n**, **p**, **r**). N.S., not significant; $^{*}P < 0.05$; $^{**}P < 0.01$; $^{***}P < 0.001$. For additional statistical information, see Supplementary data 1. Panel (**a**) Created in BioRender. Zangi, L. (2025) https://BioRender.com/scm53o8.

O.C.T. compound (Fisher Scientific), sectioned into 10μm slides using a cryostat (Leica) and processed for histology or immunofluorescence. To examine X-gal+ cell localization, X-gal (Fermentas) staining was performed according to the manufacturer's instructions.

For immunostaining, frozen sections were rinsed in PBST (PBS + 0.1% Tween-20) three times, fixed with 4% paraformaldehyde for 10 min at room temperature, permeabilized with chilled acetone for 3 min, blocked with 10% donkey serum for 20 min at room temperature, incubated with primary antibodies at 4 °C overnight and then incubated with fluorescently labeled secondary antibodies at room temperature for 30 min. All primary and secondary antibodies are listed in Supplementary Table 2. Finally, slides were mounted in Vectashield Antifade Mounting Media containing 4,6-diamidino-2-phenylindole (DAPI) counterstain (Vector Laboratories) and imaged using a confocal microscope (Olympus, Japan). To measure cardiomyocytes' cross-sectional area and nucleation, frozen sections were stained with wheat germ agglutinin (WGA) conjugated to Alexa Fluor® 488 (Invitrogen) at room temperature for 15 min before they were permeabilized, blocked and subjected to primary/secondary antibody staining as described above.

Immunofluorescence staining was quantified in 30 sections from two tissue blocks containing both sides of the anterior-septal LV scar perfused by the left anterior descending coronary artery (i.e., the border zone) and 30 sections from the region perfused by the left circumflex coronary artery (i.e., the remote zone). Randomly selected high-resolution (20× magnification,145 mm^2) images were evaluated for each section, and the results were quantified with Image J software.

Cardiac fibrosis was evaluated by quantifying five heart slices, from the apex to the papillary muscle level, taken from vehicle- or hPKM2 CM SMRT-treated groups on Day 56. This method has previously been shown to optimally represent the entire cardiac infarction[73]. Images were taken of each slice, analyzed with Image J software and presented as the ratio of scar tissue area (white) to the total area of the tissue section (red/brown) from ring 2 to 5.

Echocardiography

Animals were sedated with telazol/xylazine (4. /kg body weight), and heart rates were stably maintained at 60–80 bpm. Next, B-mode and two-dimensional M-mode images of the heart were acquired from the long-axis and short-axis views with high-resolution micro-ultrasound systems (GE LOGIQ V2 Ultrasound, GE Healthcare). Data were analyzed to calculate left ventricular ejection fraction and left ventricular fractional shortening[74].

Cardiac magnetic resonance imaging (cMRI)

Pigs were sedated with telazol/xylazine (4.4 mg/kg body weight), anesthetized with 2% inhaled isoflurane and placed in a supine position inside the MRI scanner, with ECG, respiratory and cutaneous temperature monitoring. cMRI images were acquired with a 1.5-Tesla clinical scanner (GE signa horizon software 9.1) and a phased-array 4-channel surface coil with non-breath-hold electrocardiogram (ECG) gating, as previously described[75]. The heart was scanned along two long-axis views (vertical and horizontal) and with a short-axis view set covering the entire LV from the atrioventricular valve plane to the apex. Cine imaging was performed with the following parameters: TR = 3.1 ms, TE = 1.6 ms, flip angle=45°, matrix size=224 X 128, field of view=340 × 265 mm^2, slice thickness=8 mm (with no gap between slices); 20 phases were acquired across the cardiac cycle. Infarct size was measured via late gadolinium enhancement (LGE) cMRI (0.20 mmol/kg gadopentetate dimeglumine, intravenous bolus) with the following parameters: TR = 16 ms, TE = 4 ms, TI = 150–300 ms (TI depends on how fast the contrast washes out of the myocardium), flip angle=20°, matrix size=256×148, field of view=320 × 185 mm^2, slice thickness=8 mm (with no gap between slices).

To calculate cardiac function and quantify the extent of post-infarction fibrosis, cMRI images were blind-analyzed to protect against bias while using CAAS MRV 3.4 software (Pie Medical Imaging, The Netherlands), as previously described[76]. LV endocardial and epicardial borders were manually contoured on short-axis cine images (from atrioventricular valve plane to the apex plane) at the end-diastolic and end-systolic frames to derive the left ventricular end-diastolic volume (LVEDV), end-systolic volume (LVESV), ejection fraction (EF) and stroke volume (SV). To calculate regional LV function, the left-right ventricular (LRV) junction point was further defined in all short-axis images, and the left ventricular regional wall thickening (LVWT) and radial strain (ε_{RR}) were quantified in all circumferential segments, based on the American Heart Association's 17-segment model[77]. LVWT and ε_{RR} values from 16 segments (except for apex) were plotted to generate the curve and subsequently calculate the area under the curve (AUC)[58].

Fibrotic scar was first visually identified as the gadolinium-enhanced region in a LV short-axis stack of LGE images from the atrioventricular valve plane to the apex plane and then quantified by manually adjusting a greyscale threshold to define areas of visually identified LGE. These areas were then summed to generate a total volume of LGE (Infarct Volume [ml])[58]. Infarct size (%) was defined as the proportion of the LV surface area occupied by infarct to the total LV surface area and calculated using the

following equation:

$$\text{Infarct Size}(\%) = \frac{\text{LV Scar Surface Area}}{\text{Total LV Surface Area}} \times 100\% = \frac{\sum(\text{LV Scar Arc Length} \times \text{Section thickness})}{\sum(\text{LV Circumference} \times \text{Section thickness})} \times 100\%$$

The volumes of the infarct core and the infarct gray zone (consisting of necrotic and viable myocardium surrounding the infarct core) were analyzed using the full-width half-maximum method[78].

Programmed electrical stimulation

Programmed electrical stimulation (PES) was performed as previously described[75]. Briefly, after the pig was sedated and anesthetized, an 8 F sheath was inserted in the left common carotid artery, a 7 F electrode catheter was advanced into the left ventricular apex and the heart was paced (S1) at a cycle length of 400 ms with one to three additional stimuli (S2, S3 or S4) delivered at progressively shorter intervals. S1-S2 began at 10 ms and ended at 5 ms, and the protocol was repeated for S2-S3 and S3-S4. Programmed stimulation ceased immediately after an episode of ventricular arrythmia (VA) began. VA episodes that lasted fewer than 15 heart beats were categorized as non-sustained VA, and episodes that lasted for 15 or more heart beats were categorized as sustained VA.

Statistical analysis

Statistical significance was determined by Unpaired two-tailed t-test, One or Two-way ANOVA, Tukey's Multiple Comparison Test, as detailed in respective figure legends. $p < 0.05$ was considered significant. All graphs represent average values, and values were reported as mean ± standard error of the mean. Unpaired two-tailed *t*-test was based on assumed normal distributions. Statistical analyses were performed using GraphPad Prism (version 10). Sample sizes were determined based on feasibility in large-animal studies and were not predetermined by formal power calculation. All statistical parameters, including exact *p* values, confidence, intervals, and test statistics are provided in Supplementary data 2.

Reporting summary

Further information on research design is available in the Nature Portfolio Reporting Summary linked to this article.

Data availability

The data supporting the findings of this study are available within the article and its supplementary information files. Source data for all graphs and quantifications are provided in the accompanying Source Data file. No sequencing datasets were generated. Source data are provided with this paper.

References

1. Dargie, H. Heart failure post-myocardial infarction: a review of the issues. *Heart* **91**, ii3–ii6 (2005).
2. Domenech, M., Polo-Corrales, L., Ramirez-Vick, J. E. & Freytes, D. O. Tissue engineering strategies for myocardial regeneration: acellular versus cellular scaffolds? *Tissue Eng. Part B Rev.* **22**, 438–458 (2016).
3. Chen, I. Y., Matsa, E. & Wu, J. C. Induced pluripotent stem cells: at the heart of cardiovascular precision medicine. *Nat. Rev. Cardiol.* **13**, 333–349 (2016).
4. Cannata, A., Ali, H., Sinagra, G. & Giacca, M. Gene therapy for the heart lessons learned and future perspectives. *Circ. Res.* **126**, 1394–1414 (2020).
5. Polack, F. P. et al. Safety and efficacy of the BNT162b2 mRNA Covid-19 vaccine. *N. Engl. J. Med.* **383**, 2603–2615 (2020).
6. Baden, L. R. et al. Efficacy and safety of the mRNA-1273 SARS-CoV-2 vaccine. *N. Engl. J. Med* **384**, 403–416 (2021).
7. Kariko, K. et al. Incorporation of pseudouridine into mRNA yields superior nonimmunogenic vector with increased translational capacity and biological stability. *Mol. Ther.* **16**, 1833–1840 (2008).
8. Magadum, A. et al. Ablation of a single N-glycosylation site in human FSTL 1 induces cardiomyocyte proliferation and cardiac regeneration. *Mol. Ther. Nucleic Acids* **13**, 133–143 (2018).
9. Magadum, A. et al. Pkm2 regulates cardiomyocyte cell cycle and promotes cardiac regeneration. *Circulation* **141**, 1249–1265 (2020).
10. Xiao, S. et al. STEMIN and YAP5SA synthetic modified mRNAs regenerate and repair infarcted mouse hearts. *J. Cardiovasc. Aging* **2**, 31 (2022).
11. Hadas, Y. et al. Altering sphingolipid metabolism attenuates cell death and inflammatory response after myocardial infarction. *Circulation* **141**, 916–930 (2020).
12. Magadum, A. et al. Therapeutic delivery of Pip4k2c-modified mRNA attenuates cardiac hypertrophy and fibrosis in the failing heart. *Adv. Sci. (Weinh.)* **8**, 2004661 (2021).
13. Zangi, L. et al. Insulin-like growth factor 1 receptor-dependent pathway drives epicardial adipose tissue formation after myocardial injury. *Circulation* **135**, 59–72 (2017).
14. Kaur, K. et al. Direct reprogramming induces vascular regeneration post muscle ischemic injury. *Mol. Ther.* **29**, 3042–3058 (2021).
15. Carlsson, L. et al. Biocompatible, purified VEGF-A mRNA improves cardiac function after intracardiac injection 1 week post-myocardial infarction in swine. *Mol. Ther. Methods Clin. Dev.* **9**, 330–346 (2018).
16. Zangi, L. et al. Modified mRNA directs the fate of heart progenitor cells and induces vascular regeneration after myocardial infarction. *Nat. Biotechnol.* **31**, 898–907 (2013).
17. Gan, L. M. et al. Intradermal delivery of modified mRNA encoding VEGF-A in patients with type 2 diabetes. *Nat. Commun.* **10**, 871 (2019).
18. Anttila, V. et al. Direct intramyocardial injection of VEGF mRNA in patients undergoing coronary artery bypass grafting. *Mol. Ther.* **31**, 866–874 (2023).
19. Beigi, F. et al. C3orf58, a novel paracrine protein, stimulates cardiomyocyte cell-cycle progression through the PI3K-AKT-CDK7 pathway. *Circ. Res.* **113**, 372–380 (2013).
20. Bersell, K., Arab, S., Haring, B. & Kuhn, B. Neuregulin1/ErbB4 signaling induces cardiomyocyte proliferation and repair of heart injury. *Cell* **138**, 257–270 (2009).
21. Engel, F. B. et al. p38 MAP kinase inhibition enables proliferation of adult mammalian cardiomyocytes. *Genes Dev.* **19**, 1175–1187 (2005).
22. Kuhn, B. et al. Periostin induces proliferation of differentiated cardiomyocytes and promotes cardiac repair. *Nat. Med.* **13**, 962–969 (2007).
23. Wei, K. et al. Epicardial FSTL1 reconstitution regenerates the adult mammalian heart. *Nature* **525**, 479–485 (2015).
24. Ebelt, H. et al. Directed expression of dominant-negative p73 enables proliferation of cardiomyocytes in mice. *J. Mol. Cell Cardiol.* **45**, 411–419 (2008).
25. Lin, Z. et al. Cardiac-specific YAP activation improves cardiac function and survival in an experimental murine MI model. *Circ. Res.* **115**, 354–363 (2014).
26. D'Uva, G. et al. ERBB2 triggers mammalian heart regeneration by promoting cardiomyocyte dedifferentiation and proliferation. *Nat. Cell Biol.* **17**, 627–638 (2015).
27. Heallen, T. et al. Hippo pathway inhibits Wnt signaling to restrain cardiomyocyte proliferation and heart size. *Science* **332**, 458–461 (2011).
28. Liao, H. S. et al. Cardiac-specific overexpression of cyclin-dependent kinase 2 increases smaller mononuclear cardiomyocytes. *Circ. Res.* **88**, 443–450 (2001).
29. Tang, Y. et al. MicroRNA-1 regulates cardiomyocyte apoptosis by targeting Bcl-2. *Int. Heart J.* **50**, 377–387 (2009).
30. Stahlhut, C., Suarez, Y., Lu, J., Mishima, Y. & Giraldez, A. J. miR-1 and miR-206 regulate angiogenesis by modulating VegfA expression in zebrafish. *Development* **139**, 4356–4364 (2012).
31. van Rooij, E. & Olson, E. N. MicroRNAs: powerful new regulators of heart disease and provocative therapeutic targets. *J. Clin. Invest* **117**, 2369–2376 (2007).
32. Magadum, A. et al. Specific modified mRNA translation system. *Circulation* **142**, 2485–2488 (2020).
33. Liu, S. et al. Gene therapy knockdown of Hippo signaling induces cardiomyocyte renewal in pigs after myocardial infarction. *Sci. Transl. Med.* **13**, eabd6892 (2021).

34. Baehr, A. et al. Agrin promotes coordinated therapeutic processes leading to improved cardiac repair in pigs. *Circulation* **142**, 868–881 (2020).
35. Sun, J. et al. CCND2 modified mRNA activates cell cycle of cardiomyocytes in hearts with myocardial infarction in mice and pigs. *Circ. Res.* **133**, 484–504 (2023).
36. Sultana, N. et al. Optimizing cardiac delivery of modified mRNA. *Mol. Ther.* **25**, 1306–1315 (2017).
37. Patterson, M. et al. Frequency of mononuclear diploid cardiomyocytes underlies natural variation in heart regeneration. *Nat. Genet.* **49**, 1346–1353 (2017).
38. Azoitei, N. et al. PKM2 promotes tumor angiogenesis by regulating HIF-1alpha through NF-kappaB activation. *Mol. Cancer* **15**, 3 (2016).
39. Cao, R., Brakenhielm, E., Wahlestedt, C., Thyberg, J. & Cao, Y. Leptin induces vascular permeability and synergistically stimulates angiogenesis with FGF-2 and VEGF. *Proc. Natl. Acad. Sci. USA* **98**, 6390–6395 (2001).
40. El-Sammak, H. et al. A Vegfc-Emilin2a-Cxcl8a signaling axis required for zebrafish cardiac regeneration. *Circ. Res.* **130**, 1014–1029 (2022).
41. Kalra, K., Eberhard, J., Farbehi, N., Chong, J. J. & Xaymardan, M. Role of PDGF-A/B ligands in cardiac repair after myocardial infarction. *Front Cell Dev. Biol.* **9**, 669188 (2021).
42. Rasanen, M. et al. VEGF-B promotes endocardium-derived coronary vessel development and cardiac regeneration. *Circulation* **143**, 65–77 (2021).
43. Rissanen, T. T. et al. VEGF-D is the strongest angiogenic and lymphangiogenic effector among VEGFs delivered into skeletal muscle via adenoviruses. *Circ. Res.* **92**, 1098–1106 (2003).
44. Takahashi, K. et al. Adenoviral-delivered angiopoietin-1 reduces the infarction and attenuates the progression of cardiac dysfunction in the rat model of acute myocardial infarction. *Mol. Ther.* **8**, 584–592 (2003).
45. Brindle, N. P., Saharinen, P. & Alitalo, K. Signaling and functions of angiopoietin-1 in vascular protection. *Circ. Res.* **98**, 1014–1023 (2006).
46. Collen, A. et al. VEGFA mRNA for regenerative treatment of heart failure. *Nat. Rev. Drug Discov.* **21**, 79–80 (2022).
47. Glinton, K. E. et al. Macrophage-produced VEGFC is induced by efferocytosis to ameliorate cardiac injury and inflammation. *J. Clin. Investig.* **132**, e140685–e140685 (2022).
48. Hsieh, P. C., Davis, M. E., Gannon, J., MacGillivray, C. & Lee, R. T. Controlled delivery of PDGF-BB for myocardial protection using injectable self-assembling peptide nanofibers. *J. Clin. Invest* **116**, 237–248 (2006).
49. Pajula, J. et al. Adenoviral VEGF-D(DeltaN DeltaC) gene therapy for myocardial ischemia. *Front Bioeng. Biotechnol.* **10**, 999226 (2022).
50. Smith, C. C. et al. Leptin-induced cardioprotection involves JAK/STAT signaling that may be linked to the mitochondrial permeability transition pore. *Am. J. Physiol. Heart Circul. Physiol.* **299**, H1265–H1270 (2010).
51. Wolpert, E. Z., Grufman, P., Sandberg, J. K., Tegnesjo, A. & Karre, K. Immunodominance in the CTL response against minor histocompatibility antigens: interference between responding T cells, rather than with presentation of epitopes. *J. Immunol.* **161**, 4499–4505 (1998).
52. Murphy, S. P., Ibrahim, N. E. & Januzzi, J. L. Jr. Heart failure with reduced ejection fraction: a review. *JAMA* **324**, 488–504 (2020).
53. Sondergaard, L. V., Dagnaes-Hansen, F. & Herskin, M. S. Welfare assessment in porcine biomedical research—suggestion for an operational tool. *Res Vet. Sci.* **91**, e1–e9 (2011).
54. Porrello, E. R. et al. Transient regenerative potential of the neonatal mouse heart. *Science* **331**, 1078–1080 (2011).
55. Zhu, W. et al. Regenerative potential of neonatal porcine hearts. *Circulation* **138**, 2809–2816 (2018).
56. Huser, D. et al. Integration preferences of wildtype AAV-2 for consensus rep-binding sites at numerous loci in the human genome. *PLoS Pathog.* **6**, e1000985 (2010).
57. Nowrouzi, A. et al. Integration frequency and intermolecular recombination of rAAV vectors in non-human primate skeletal muscle and liver. *Mol. Ther.* **20**, 1177–1186 (2012).
58. Gabisonia, K. et al. MicroRNA therapy stimulates uncontrolled cardiac repair after myocardial infarction in pigs. *Nature* **569**, 418–422 (2019).
59. Sahoo, S., Kariya, T. & Ishikawa, K. Targeted delivery of therapeutic agents to the heart. *Nat. Rev. Cardiol.* **18**, 389–399 (2021).
60. Zak, M. M. et al. Modified mRNA formulation and stability for cardiac and skeletal muscle delivery. *Pharmaceutics* **15**, 2176 (2023).
61. Fukuda, R. et al. Metabolic modulation regulates cardiac wall morphogenesis in zebrafish. *Elife* **8**, e50161 (2019).
62. Ni, L. et al. Pyruvate kinase M2 protects heart from pressure overload-induced heart failure by phosphorylating RAC1. *J. Am. Heart Assoc.* **11**, e024854 (2022).
63. Shi, J., Yang, X., Yang, D., Li, Y. & Liu, Y. Pyruvate kinase isoenzyme M2 expression correlates with survival of cardiomyocytes after allogeneic rat heterotopic heart transplantation. *Pathol. Res. Pract.* **211**, 12–19 (2015).
64. Gao, X., Wang, H., Yang, J. J., Liu, X. & Liu, Z. R. Pyruvate kinase M2 regulates gene transcription by acting as a protein kinase. *Mol. Cell* **45**, 598–609 (2012).
65. Luo, W. & Semenza, G. L. Pyruvate kinase M2 regulates glucose metabolism by functioning as a coactivator for hypoxia-inducible factor 1 in cancer cells. *Oncotarget* **2**, 551–556 (2011).
66. Lv, X. et al. The role of hypoxia-inducible factors in tumor angiogenesis and cell metabolism. *Genes Dis.* **4**, 19–24 (2017).
67. Zhang, Z. et al. PKM2, function and expression and regulation. *Cell Biosci.* **9**, 52 (2019).
68. Souders, C. A. et al. c-Myc is required for proper coronary vascular formation via cell- and gene-specific signaling. *Arteriosclerosis Thrombosis Vasc. Biol.* **32**, 1308–1319 (2012).
69. Gu, J. et al. The role of PKM2 nuclear translocation in the constant activation of the NF-kappaB signaling pathway in cancer-associated fibroblasts. *Cell Death Dis.* **12**, 291 (2021).
70. Wang, J. H., Gessler, D. J., Zhan, W., Gallagher, T. L. & Gao, G. Adeno-associated virus as a delivery vector for gene therapy of human diseases. *Signal Transduct. Target Ther.* **9**, 78 (2024).
71. Zak M. M., Zangi L. Lipid Nanoparticles for Organ-Specific mRNA Therapeutic Delivery. *Pharmaceutics* **13**, 1675 (2021).
72. Yoo, J. & Zangi, L. Optimization of synthesis of modified mRNA. *Methods Mol. Biol.* **2573**, 77–87 (2022).
73. Takagawa, J. et al. Myocardial infarct size measurement in the mouse chronic infarction model: comparison of area- and length-based approaches. *J. Appl Physiol. (1985)* **102**, 2104–2111 (2007).
74. Zhao, M. et al. Cyclin D2 overexpression enhances the efficacy of human induced pluripotent stem cell-derived cardiomyocytes for myocardial repair in a swine model of myocardial infarction. *Circulation* **144**, 210–228 (2021).
75. Gao, L. et al. Exosomes secreted by hiPSC-derived cardiac cells improve recovery from myocardial infarction in swine. *Sci. Transl. Med.* **12**, eaay1318 (2020).
76. Polacin, M. et al. Segmental strain analysis for the detection of chronic ischemic scars in non-contrast cardiac MRI cine images. *Sci. Rep.* **11**, 12376 (2021).
77. Cerqueira, M. D. et al. Standardized myocardial segmentation and nomenclature for tomographic imaging of the heart. A statement for healthcare professionals from the Cardiac Imaging Committee of the Council on Clinical Cardiology of the American Heart Association. *Circulation* **105**, 539–542 (2002).
78. Schmidt, A. et al. Infarct tissue heterogeneity by magnetic resonance imaging identifies enhanced cardiac arrhythmia

susceptibility in patients with left ventricular dysfunction. *Circulation* **115**, 2006–2014 (2007).

Acknowledgements

This work was funded by a NantRNA sponsor research agreement with Mount Sinai as well as NIH grants R01 HL142768-01 and R01 HL149137-01 (to L.Z.). This work was also supported by the following funding sources: NIH RO1s, HL114120, HL 131017, HL 149137, NIH UO1 HL134764, NIH PO1 HL160476 (to J.Z.); American Heart Association 23PRE1025367 (to J.S.).

Author contributions

J.S., J.Z. and L.Z. conceived and designed the project. J.S., Y.W., M.A., R.C.M., A.A.K., M.M.Z., J.Y., G.M., H.L., Y.L. and G.P.W. acquired and analyzed data. M.A., P.S.S., J.S., Y.W., H.A.S., J.Z. and L.Z. wrote and revised the manuscript.

Competing interests

L. Zangi is an inventor of Issued patents, titled Cell-specific expression of modRNA (PCT/US2017/052035; Issued patents in US, EP, AU, UK, SP, JP), that cover the use of hPKM2 CM SMRTs to promote cardiac repair after MI. All authors declare no competing interests.

Data sharing statement

All modified mRNA (modRNA) vectors containing genes of interest noted in this paper will be made available to other investigators. My institution and I will adhere to the NIH Grants Policy on Sharing of Unique Research Resources including the "Sharing of Biomedical Research Resources: Principles and Guidelines for Recipients of NIH Grants and Contracts" issued in December 1999. Specifically, material transfers will be made with no more restrictive terms than in the Simple Letter Agreement or the UBMTA and without reach-through requirements. Should any intellectual property arise which requires a patent, we would ensure that the technology remains widely available to the research community, in accordance with the NIH Principles and Guidelines.

Additional information

Supplementary information The online version contains supplementary material available at https://doi.org/10.1038/s41467-025-65344-4.

Correspondence and requests for materials should be addressed to Jianyi Zhang or Lior Zangi.

Peer review information *Nature Communications* thanks Qing-Dong Wang, and the other, anonymous, reviewers for their contribution to the peer review of this work. A peer review file is available.